

Article

# Critical Current and Pinning Features of a CaKFe<sub>4</sub>As<sub>4</sub> Polycrystalline Sample

Armando Galluzzi<sup>1,2,\*</sup>, Antonio Leo<sup>1,2</sup>, Andrea Masi<sup>3,4</sup>, Francesca Varsano<sup>3</sup>, Angela Nigro<sup>1,2</sup>, Gaia Grimaldi<sup>2</sup> and Massimiliano Polichetti<sup>1,2,\*</sup>

<sup>1</sup> Department of Physics “E.R. Caianiello”, University of Salerno, Via Giovanni Paolo II 132, Fisciano, I-84084 Salerno, Italy; aleo@unisa.it (A.L.); anigro@unisa.it (A.N.)

<sup>2</sup> CNR-SPIN Salerno, Via Giovanni Paolo II 132, Fisciano, I-84084 Salerno, Italy; gaia.grimaldi@spin.cnr.it

<sup>3</sup> ENEA, Via Anguillarese 301, I-00123 Roma, Italy; andrea.masi@enea.it (A.M.); francesca.varsano@enea.it (F.V.)

<sup>4</sup> Dipartimento di Ingegneria, Università degli Studi Roma Tre, Via Vito Volterra 62, I-00146 Roma, Italy

\* Correspondence: agalluzzi@unisa.it (A.G.); mpolichetti@unisa.it (M.P.)

**Abstract:** We analyze the magnetic behavior of a CaKFe<sub>4</sub>As<sub>4</sub> polycrystalline sample fabricated by a mechanochemically assisted synthesis route. By means of DC magnetization (M) measurements as a function of the temperature (T) and DC magnetic field (H) we study its critical parameters and pinning features. The critical temperature T<sub>c</sub> has been evaluated by M(T) curves performed in Zero Field Cooling–Field Cooling conditions. These curves show the presence of a little magnetic background for temperatures above T<sub>c</sub>, as also confirmed by the hysteresis loops M(H). Starting from the M(H) curves, the critical current density J<sub>c</sub> of the sample has been calculated as a function of the field at different temperatures in the framework of the Bean critical state model. The J<sub>c</sub>(H) values are in line with the ones reported in the literature for this typology of samples. By analyzing the temperature dependence of the critical current density J<sub>c</sub>(T) at different magnetic fields, it has been found that the sample is characterized by a strong type pinning regime. This sample peculiarity can open perspectives for future improvement in the fabrication of this material.

**Keywords:** iron-based superconductors; 1144 IBS family; DC magnetic properties; pinning properties; pinning force analysis; magnetism and superconductivity



**Citation:** Galluzzi, A.; Leo, A.; Masi, A.; Varsano, F.; Nigro, A.; Grimaldi, G.; Polichetti, M. Critical Current and Pinning Features of a CaKFe<sub>4</sub>As<sub>4</sub> Polycrystalline Sample. *Materials* **2021**, *14*, 6611. <https://doi.org/10.3390/ma14216611>

Academic Editor: Guang-Han Cao

Received: 19 October 2021

Accepted: 1 November 2021

Published: 3 November 2021

**Publisher’s Note:** MDPI stays neutral with regard to jurisdictional claims in published maps and institutional affiliations.



**Copyright:** © 2021 by the authors. Licensee MDPI, Basel, Switzerland. This article is an open access article distributed under the terms and conditions of the Creative Commons Attribution (CC BY) license (<https://creativecommons.org/licenses/by/4.0/>).

## 1. Introduction

Until 2016, with the discovery of the 1144 Iron-Based superconductors (IBSs) family [1], the 122 and 11 IBS families have been the most studied due to their low anisotropy values, high values of critical current density J<sub>c</sub>, irreversibility field and upper critical field [2–10]. In this framework, the 1144 family [1] attracted significant interest in recent years due to the stoichiometric nature of its layered structure. This group of IBSs shares in fact key structural elements with the 122 family [11], well known for the optimum results obtained following their application in the production of superconducting wires [12]. The 1144 and 122 compounds are both characterized by the intercalation of mixed Alkaline (A) or Alkaline Earth (AE) ions between Fe-As planes, with the difference that in the 1144 structure A and AE elements do not mix in the same planes. The rigid alternation of A and AE elements gives rise to the formation of stoichiometric superconductors characterized by hole doping levels close to the optimal 0.4 observed in common 122 IBS, with critical temperatures above 35 K and high critical currents.

Regarding the superconducting critical currents, it has been observed in 1144 single crystals that the alternation of the elements in the intercalating planes can give rise to the formation of peculiar lattice defects that resemble stacking faults observed in cuprates [13–15]. The presence of these defects has been associated with the high critical currents observed in 1144 single crystals and with peculiar second magnetization peak phenomena observed in

such crystals, and linked to the material pinning dynamics. In this work, we have analyzed the critical current density as a function of field and temperature together with the pinning features of a polycrystalline sample. Specifically, after having obtained the  $T_c$  of the sample, we have extracted the  $J_c(H)$  curves starting from the  $M(H)$  loops comparing their values with the literature. After that, by analyzing the  $J_c(T)$  curves' behavior and the pinning force density as a function of the reduced field  $F_p(h)$  curves, a strong pinning regime has been identified. The obtained results show that the sample can be considered for high-power applications due to its strong pinning behavior and to the possibility to enhance the critical current density values by improving the fabrication processes.

## 2. Materials and Methods

We have analyzed a disk-shaped pellet with diameter and thickness equal to 3 mm and 0.65 mm, respectively. The polycrystalline sample was obtained via a mechanochemically assisted synthesis route [16]. Briefly, elemental powders were subjected to a milling treatment using a steel vial and steel balls in a 30:1 ball to powder mass ratio for 5 h. The pressed powders were then subjected to thermal treatment for 10 h at 750 °C, adopting a 10 °C/min heating rate and a 5 °C/min cooling rate. With respect to our previous work, a slight imbalance in the starting Ca:K ratio was introduced in order to minimize K-122 phase segregation [17] starting thus from a nominal Ca:K:Fe:As = 1.2:1.18:3.75:4 atomic ratio. XRD diffraction patterns (data not shown) show the distinctive peaks of the  $p4/mmm$  1144 phase [1] as in our previous work [17] and do not highlight significant presence of secondary phases (only traces of K-122 and CaO are evident). The sample has been characterized by means of DC magnetic measurements applied perpendicularly to the disk surface. The temperature and field dependence of the DC magnetization  $M(T)$  and  $M(H)$ , respectively, has been measured by means of a QD PPMS doted of a VSM insert. To avoid the effect on the sample response due to the residual trapped field inside the PPMS DC magnet [18], this field was reduced below  $1 \times 10^{-4}$  T [19]. The sample has been cooled down to 2.5 K in zero field, then the H has been applied and the data have been gained for rising temperatures (Zero Field Cooling) up to 300 K. Then, the sample has been cooled again during the acquisition of the Field Cooling magnetization. For what concerns the  $M(H)$  measurements, the sample has been cooled to the interested temperature in zero field. Then, H was ramped up to +9 T, down to -9 T, and to +9 T again for acquiring the complete  $M(H)$  loops [20].

## 3. Results and Discussion

To obtain the  $T_c$  of the sample, a  $M(T)$  measurement has been made in Zero Field Cooling (ZFC)-Field Cooling (FC) conditions by using 0.01 T. The  $M(T)$  at  $H = 0.01$  T is reported in Figure 1. The  $T_c$  has been individuated as the beginning of the ZFC  $M(T)$  transition (see inset of Figure 1). This value is approximately 35 K and it is consistent with the values reported in the literature [1,21,22]. It is worth noting the presence of a slight non-zero signal above  $T_c$  in the ZFC curve as already reported in other works on iron-based systems [23–26], which can be limited by improving the fabrication processes [26–28].

The  $M(H)$  measurements have been performed at different temperatures in the range between 5 K and 40 K (see Figure 2). The decrease of the hysteresis areas with increasing temperature and the shape of  $M(H)$  loops imply the existence of flux pinning centers. Moreover, the not perfect symmetry of the superconducting hysteresis loops indicates the possible presence of surface barriers [29,30].

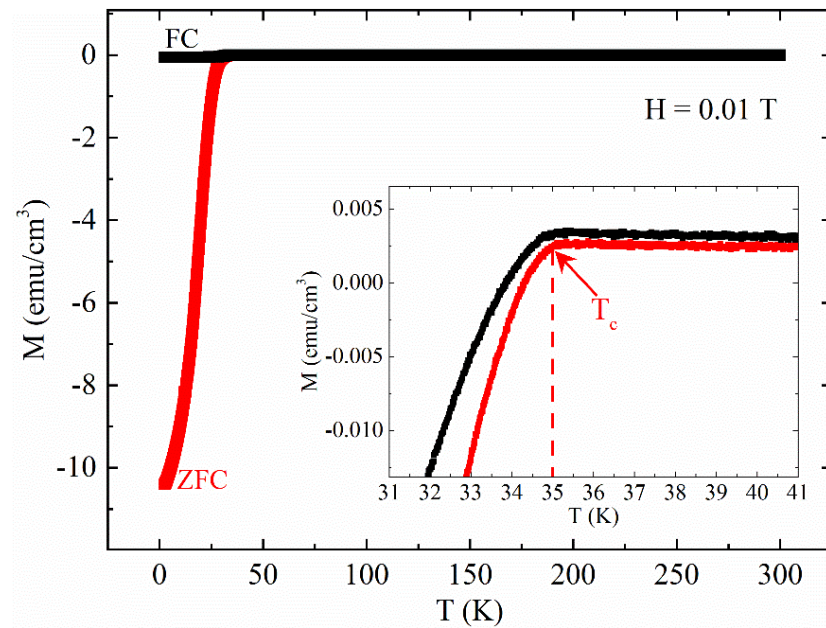


**Figure 1.** Magnetization versus temperature  $M(T)$  measured in ZFC-FC conditions at  $H = 0.01$  T. Inset:  $T_c$  is indicated by a red arrow.

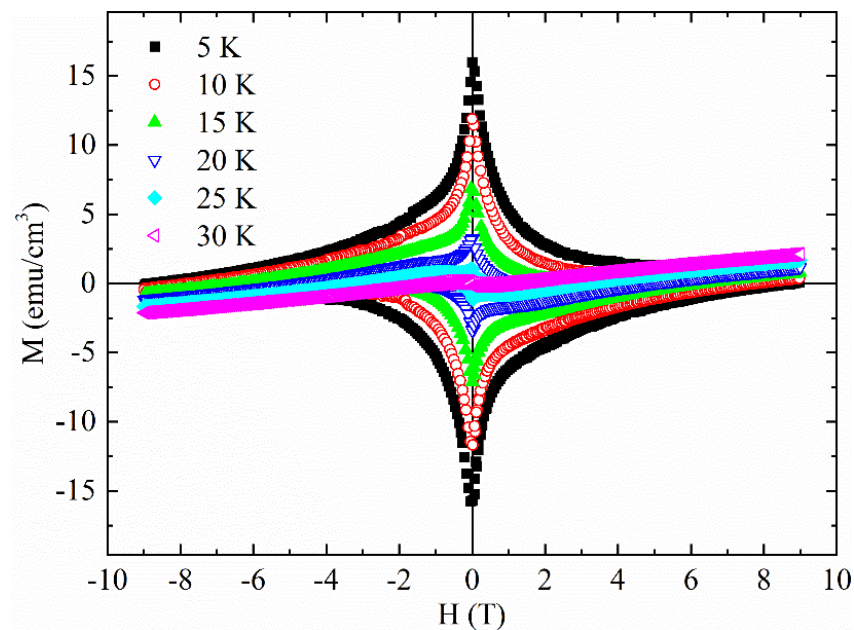


**Figure 2.** Magnetization versus field at different temperatures below  $T_c$ .

It is visible a slight tilt of the curves probably due to the presence of a magnetic background or to magnetic impurities already detected in ZFC curve of Figure 1. In this framework, Figure 3 shows the  $M(H)$  curve at  $T = 40$  K. At this temperature, the sample is in the normal state, so approximately this curve represents the magnetic background of the sample, which coexists with superconducting signal at lower temperatures  $T < T_c$ . In particular, the coercive field is  $\approx 100$  Oe.

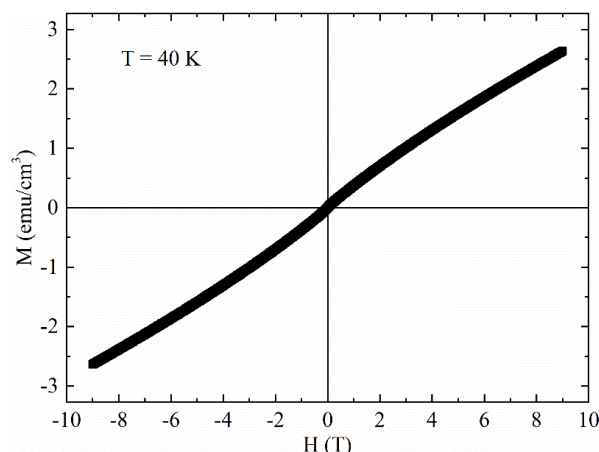


**Figure 3.** Magnetic hysteresis loop at  $T = 40$  K.

To analyze the transport and pinning properties of the sample, the critical current densities as a function of the magnetic field  $J_c(H)$  and the temperature  $J_c(T)$  have been studied. In particular, the  $J_c(H)$  at different temperatures have been calculated by means of the formula [31,32]:

$$J_c = \frac{30\Delta M}{d}, \quad (1)$$

where  $\Delta M = M_{dn} - M_{up}$  is the difference between the magnetization measured for decreasing ( $M_{dn}$ ) and increasing ( $M_{up}$ ) applied field, respectively, and  $d$  is the diameter. The  $\Delta M$  is expressed in  $\text{emu}/\text{cm}^3$ . In Figure 4, the obtained  $J_c(H)$  curves have been reported for different temperatures. The obtained  $J_c$  values are in agreement with the ones reported in the literature for other polycrystalline  $\text{CaKFe}_4\text{As}_4$  samples [16,22,33].

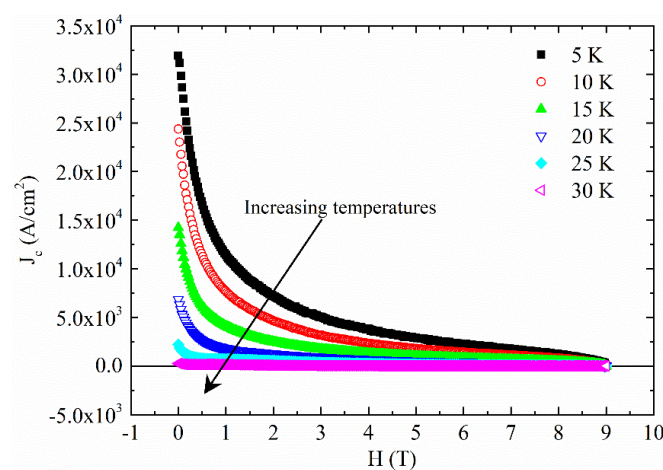


**Figure 4.**  $J_c$  versus field at different temperatures.

Now, by fixing the field and by cutting the  $J_c(H)$  obtained at different temperatures and reported in Figure 4, the  $J_c(T)$  curves have been constructed and analyzed by using different equations reported in the literature describing different pinning models [34–41]. In all the field ranges, the best fit of the  $J_c(T)$  curves has been obtained with equation considering the presence of strong pinning defects [42–45]

$$J_c^{\text{str}}(T) = J_c^{\text{str}}(0) e^{-3(T/T^*)^2}, \quad (2)$$

where  $J_c^{\text{str}}(T)$  is the temperature dependence of  $J_c$  in the framework of strong pinning regime,  $J_c^{\text{str}}(0)$  is  $J_c$  at  $T = 0$  K and  $T^*$  characterizes the vortex pinning by strong defect centers. The  $J_c(T)$  curves fit for different magnetic fields is reported in Figure 5. It can be

noted how the strong pinning model fits well our experimental data for all the considered field ranges. From these fits, the critical current density values at  $T = 0$  K has been extracted as indicated with a red open circle in each of the panels of Figure 5, while  $T^* \approx 24$  K for all the fits. Collecting these values, the  $J_c(H)$  at  $T = 0$  K has been obtained and reported in Figure 6. This curve has been fitted with several critical state models describing the field dependence of  $J_c$  [46–51]. The best fit has been obtained by using the Kim critical state model [47,48]

$$J_c(H) = \frac{J_c(0)}{1 + H/B_k}, \quad (3)$$

where  $J_c(0)$  is the value of  $J_c$  at  $H = 0$  K and  $B_k$  is a parameter associated with the internal field. From the fit,  $B_k \approx 0.63$  T and the  $J_c$  at  $T = 0$  K and  $H = 0$  T,  $J_c(0,0)$ , can be obtained:  $J_c(0,0) = 36,800$  A/cm<sup>2</sup>.

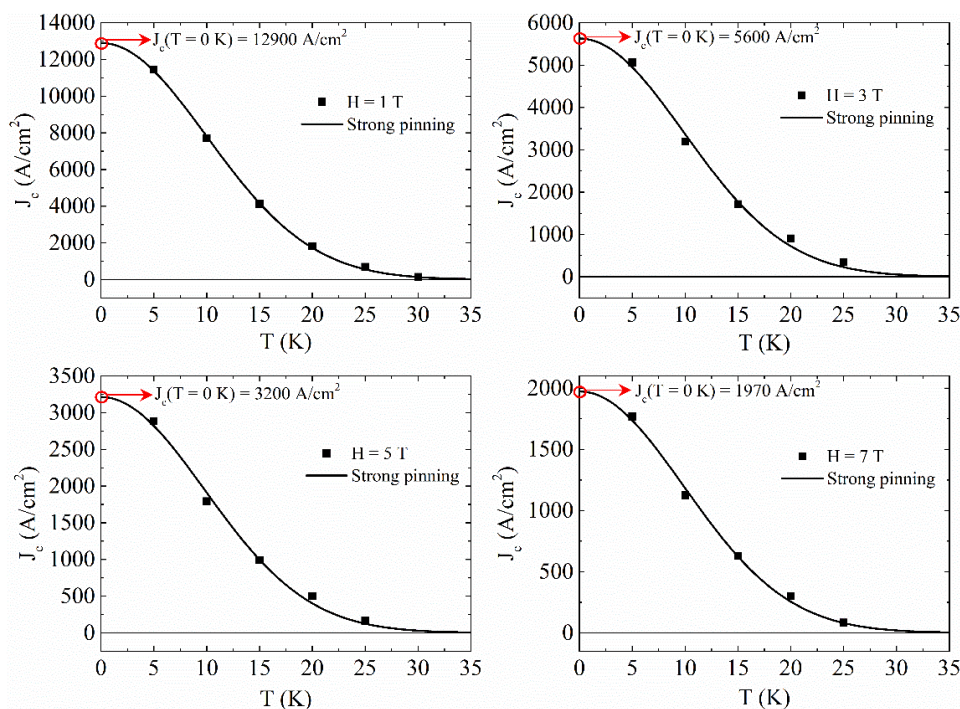


**Figure 5.** Temperature dependence of  $J_c$  at different applied magnetic fields fitted with strong pinning model (black solid line).

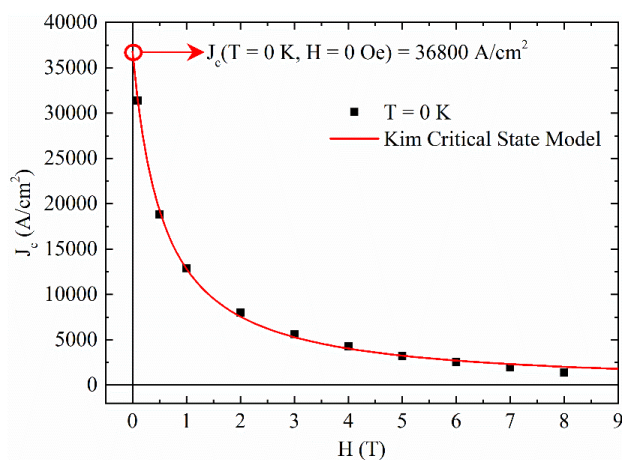


**Figure 6.**  $J_c$  at  $T = 0$  K as a function of the magnetic field has been reported together with the fit with the Kim critical state model (red solid line).

The fit of the  $J_c(T)$  curves by means of several pinning models is a powerful tool for discovering the pinning regime acting in the sample. On the other hand, it does not give specific information on the pinning defect type present in the sample. In this context, for deepening this aspect, it is helpful to study the behavior of the normalized pinning force density  $F_p/F_p^{\max}$  as a function of the reduced magnetic field  $h = H/H_{\text{irr}}$  (where  $H_{\text{irr}}$  is the irreversibility field) by using the Dew–Hughes model [29]:

$$\frac{F_p}{F_p^{\max}} = Ch^p(1-h)^q, \quad (4)$$

where  $C$  is a proportionality constant, and  $p$  and  $q$  are fitting parameters that allow individuating the pinning defect type of the material. Equation (4) considers a maximum in the  $F_p/F_p^{\max}$  vs.  $h$  behavior. In particular, for  $\delta l$  pinning the  $F_p/F_p^{\max}$  maximum occurs at  $h_{\max} = 0.33$  with  $p = 1$  and  $q = 2$  in the case of point pins, at  $h_{\max} = 0.20$  with  $p = 0.5$  and  $q = 2$  in the case of surface pins, while no maximum occurs with  $p = 0$  and  $q = 2$  in the case of volume pinning [29]. For  $\delta T_c$  pinning, the maximum is expected for higher  $h$  than  $\delta l$  pinning [29]. In our case,  $H_{\text{irr}} = 6$  T has been determined by taking the value of the magnetic field at which  $J_c \approx 10$  A/cm<sup>2</sup> [52]. In Figure 7, the fit of  $F_p/F_p^{\max}$  vs.  $h$  curve with Equation (4) has been reported.

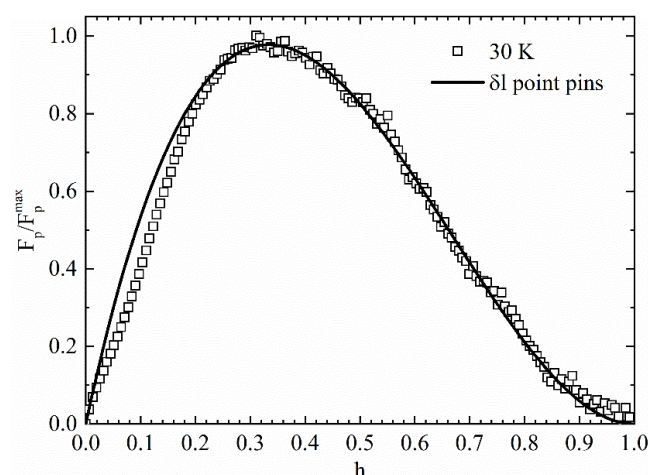


**Figure 7.** Normalized pinning force density as a function of the reduced magnetic field  $h = H/H_{\text{irr}}$  at  $T = 30$  K fitted with Equation (4). Fit details are reported in the text.

The fit of Equation (4) with the experimental data gives  $h_{\max} \approx 0.33$ ,  $p \approx 1$  and  $q \approx 2$ , thus indicating that the point pins dominate the pinning mechanism inside our sample at  $T = 30$  K. This has also been verified for other temperatures. It is worth to underline that this result is in agreement with the fit of the  $J_c(H)$  at  $T = 0$  K performed in Figure 6. In fact, the Kim critical state model can describe a superconductor having a homogeneous point defects distribution. In our opinion, since strong pinning regime has been found characterizing the sample, better current transport properties could be achieved with a better connection among the grains of our polycrystalline sample, which often is the key to enhancing the critical current density values in this class of superconductors [53–57].

#### 4. Conclusions

We have studied the magnetic response of a  $\text{CaKFe}_4\text{As}_4$  polycrystalline sample by using DC magnetization measurements as a function of the temperature and magnetic field. From the analysis of the Zero Field Cooling  $M(T)$  curve,  $T_c$  has been found equal to 35 K. A slight magnetic background has been found in the  $M(T)$  and  $M(H)$  curves for  $T > T_c$ . In particular, due to the magnetic contribution, the superconducting hysteresis loops have shown a slight tilt, while the  $M(H)$  at 40 K has shown a coercive field different from zero, suggesting the presence of a ferro/ferrimagnetic phase or of magnetic impurities inside

the sample. However, the magnetic contribution did not affect the critical current density calculated starting from the  $M(H)$  curves. In particular, the field dependence of the critical current density  $J_c(H)$  has shown values in agreement with other polycrystalline samples present in the literature. By analyzing the  $J_c(T)$  curves at different magnetic fields and the  $F_p(h)$ , it has been found that a strong pinning regime characterized by point pins acts in the sample for all the field ranges. Finally, the  $J_c(H)$  at  $T = 0$  K has been obtained and fitted in the framework of the Kim critical state model coherently with the presence of point pins in the sample. Although the current transport capabilities are not excellent, the obtained results suggest that the enhancement of the number of the strong defects and a better connection among grains, which can be obtained by manipulating the fabrication processes, can significantly increase the critical current density values of the sample.

**Author Contributions:** Conceptualization, A.G., A.L., A.M. and F.V.; methodology, A.G. and A.L.; validation, A.G., A.L. and M.P.; formal analysis, A.G. and A.L.; investigation, A.G., A.L., A.M., A.N. and G.G.; data curation, A.G., A.L., A.M. and F.V.; writing—original draft preparation, A.G. and A.L.; writing—review and editing, A.M., F.V., A.N., G.G. and M.P.; visualization, A.N., G.G. and M.P.; supervision, G.G. and M.P.; project administration, G.G. and M.P. All authors have read and agreed to the published version of the manuscript.

**Funding:** This research received no external funding.

**Institutional Review Board Statement:** Not applicable.

**Informed Consent Statement:** Not applicable.

**Data Availability Statement:** The data sets that support the findings in this study are available from the corresponding author upon reasonable request.

**Conflicts of Interest:** The authors declare no conflict of interest.

## References

1. Iyo, A.; Kawashima, K.; Kinjo, T.; Nishio, T.; Ishida, S.; Fujihisa, H.; Gotoh, Y.; Kihou, K.; Eisaki, H.; Yoshida, Y. New-Structure-Type Fe-Based Superconductors:  $\text{CaAFe}_4\text{As}_4$  ( $A = \text{K, Rb, Cs}$ ) and  $\text{SrAFe}_4\text{As}_4$  ( $A = \text{Rb, Cs}$ ). *J. Am. Chem. Soc.* **2016**, *138*, 3410–3415. [[CrossRef](#)] [[PubMed](#)]
2. Yuan, H.Q.; Singleton, J.; Balakirev, F.F.; Baily, S.A.; Chen, G.F.; Luo, J.L.; Wang, N.L. Nearly isotropic superconductivity in  $(\text{Ba,K})\text{Fe}_2\text{As}_2$ . *Nature* **2009**, *457*, 565–568. [[CrossRef](#)]
3. Yamamoto, A.; Jaroszynski, J.; Tarantini, C.; Balicas, L.; Jiang, J.; Gurevich, A.; Larbalestier, D.C.; Jin, R.; Sefat, A.S.; McGuire, M.A.; et al. Small anisotropy, weak thermal fluctuations, and high field superconductivity in Co-doped iron pnictide. *Cit. Appl. Phys. Lett.* **2009**, *94*, 062511. [[CrossRef](#)]
4. Grimaldi, G.; Leo, A.; Martucciello, N.; Braccini, V.; Bellingeri, E.; Ferdeghini, C.; Galluzzi, A.; Polichetti, M.; Nigro, A.; Villégier, J.-C.; et al. Weak or Strong Anisotropy in Fe(Se,Te) Superconducting Thin Films Made of Layered Iron-Based Material? *IEEE Trans. Appl. Supercond.* **2019**, *29*, 1–4. [[CrossRef](#)]
5. Leo, A.; Braccini, V.; Bellingeri, E.; Ferdeghini, C.; Galluzzi, A.; Polichetti, M.; Nigro, A.; Pace, S.; Grimaldi, G. Anisotropy effects on the quenching current of Fe(Se,Te) Thin Films. *IEEE Trans. Appl. Supercond.* **2018**, *28*, 8234633. [[CrossRef](#)]
6. Galluzzi, A.; Buchkov, K.; Nazarova, E.; Tomov, V.; Grimaldi, G.; Leo, A.; Pace, S.; Polichetti, M. Transport properties and high upper critical field of a Fe(Se,Te) iron based superconductor. *Eur. Phys. J. Spec. Top.* **2019**, *228*, 725–731. [[CrossRef](#)]
7. Hosono, H.; Yamamoto, A.; Hiramatsu, H.; Ma, Y. Recent advances in iron-based superconductors toward applications. *Mater. Today* **2018**, *21*, 278–302. [[CrossRef](#)]
8. Galluzzi, A.; Buchkov, K.; Nazarova, E.; Leo, A.; Grimaldi, G.; Pace, S.; Polichetti, M. Silver doping effects on irreversibility field and pinning energy of a FeSe iron based superconductor. *J. Phys. Conf. Ser.* **2020**, *1548*, 012024. [[CrossRef](#)]
9. Galluzzi, A.; Buchkov, K.M.; Nazarova, E.; Tomov, V.; Grimaldi, G.; Leo, A.; Pace, S.; Polichetti, M. Pinning energy and anisotropy properties of a Fe(Se,Te) iron based superconductor. *Nanotechnology* **2019**, *30*, 254001. [[CrossRef](#)] [[PubMed](#)]
10. Galluzzi, A.; Buchkov, K.; Tomov, V.; Nazarova, E.; Kovacheva, D.; Leo, A.; Grimaldi, G.; Pace, S.; Polichetti, M. Mixed state properties of iron based Fe(Se,Te) superconductor fabricated by Bridgman and by self-flux methods. *J. Appl. Phys.* **2018**, *123*, 233904. [[CrossRef](#)]
11. Rotter, M.; Tegel, M.; Johrendt, D. Superconductivity at 38 K in the iron arsenide  $(\text{Ba}_{1-x}\text{K}_x)\text{Fe}_2\text{As}_2$ . *Phys. Rev. Lett.* **2008**, *101*, 107006. [[CrossRef](#)]
12. Yao, C.; Ma, Y. Recent breakthrough development in iron-based superconducting wires for practical applications. *Supercond. Sci. Technol.* **2019**, *32*, 023002. [[CrossRef](#)]

13. Ishida, S.; Iyo, A.; Ogino, H.; Eisaki, H.; Takeshita, N.; Kawashima, K.; Yanagisawa, K.; Kobayashi, Y.; Kimoto, K.; Abe, H.; et al. Unique defect structure and advantageous vortex pinning properties in superconducting  $\text{CaKFe}_4\text{As}_4$ . *npj Quantum Mater.* **2019**, *4*, 27. [[CrossRef](#)]
14. Pyon, S.; Takahashi, A.; Veshchunov, I.; Tamegai, T.; Ishida, S.; Iyo, A.; Eisaki, H.; Imai, M.; Abe, H.; Terashima, T.; et al. Large and significantly anisotropic critical current density induced by planar defects in  $\text{CaKFe}_4\text{As}_4$  single crystals. *Phys. Rev. B* **2019**, *99*, 104506. [[CrossRef](#)]
15. Wang, C.; He, T.; Han, Q.; Fan, C.; Tang, Q.; Chen, D.; Lei, Q.; Sun, S.; Li, Y.; Yu, B. Novel sample-thickness-dependent flux pinning behaviors of  $\text{KFe}_2\text{As}_2$  intercalations in  $\text{CaKFe}_4\text{As}_4$  single crystals. *Supercond. Sci. Technol.* **2021**, *34*, 055001. [[CrossRef](#)]
16. Masi, A.; Angrisani Armenio, A.; Celentano, G.; La Barbera, A.; Rufoloni, A.; Silva, E.; Vannozzi, A.; Varsano, F. Mechanochemically assisted low temperature synthesis route of the 1144 Ca-K Iron Based Superconductor. *Supercond. Sci. Technol.* **2020**, *33*, 74003. [[CrossRef](#)]
17. Masi, A.; Angrisani Armenio, A.; Celentano, G.; La Barbera, A.; Rufoloni, A.; Silva, E.; Vannozzi, A.; Varsano, F. The role of chemical composition in the synthesis of Ca/K-1144 iron based superconductors. *J. Alloys. Compd.* **2021**, *869*, 159202. [[CrossRef](#)]
18. Polichetti, M.; Galluzzi, A.; Buchkov, K.; Tomov, V.; Nazarova, E.; Leo, A.; Grimaldi, G.; Pace, S. A precursor mechanism triggering the second magnetization peak phenomenon in superconducting materials. *Sci. Rep.* **2021**, *11*, 7247. [[CrossRef](#)]
19. Galluzzi, A.; Mancusi, D.; Cirillo, C.; Attanasio, C.; Pace, S.; Polichetti, M. Determination of the Transition Temperature of a Weak Ferromagnetic Thin Film by Means of an Evolution of the Method Based on the Arrott Plots. *J. Supercond. Nov. Magn.* **2018**, *31*, 1127–1132. [[CrossRef](#)]
20. Galluzzi, A.; Buchkov, K.; Tomov, V.; Nazarova, E.; Leo, A.; Grimaldi, G.; Nigro, A.; Pace, S.; Polichetti, M. Second Magnetization Peak Effect in a  $\text{Fe}(\text{Se},\text{Te})$  iron based superconductor. *J. Phys. Conf. Ser.* **2019**, *1226*, 012012. [[CrossRef](#)]
21. Meier, W.R.; Kong, T.; Bud'Ko, S.L.; Canfield, P.C. Optimization of the crystal growth of the superconductor  $\text{CaKFe}_4\text{As}_4$  from solution in the  $\text{FeAs}-\text{CaFe}_2\text{As}_2-\text{KFe}_2\text{As}_2$  system. *Phys. Rev. Mater.* **2017**, *1*, 013401. [[CrossRef](#)]
22. Singh, S.J.; Bristow, M.; Meier, W.R.; Taylor, P.; Blundell, S.J.; Canfield, P.C.; Coldea, A.I. Ultrahigh critical current densities, the vortex phase diagram, and the effect of granularity of the stoichiometric high-Tc superconductor  $\text{CaKFe}_4\text{As}_4$ . *Phys. Rev. Mater.* **2018**, *2*, 74802. [[CrossRef](#)]
23. Cimberle, M.R.; Canepa, F.; Ferretti, M.; Martinelli, A.; Palenzona, A.; Siri, A.S.; Tarantini, C.; Tropeano, M.; Ferdeghini, C. Magnetic characterization of undoped and 15%F-doped  $\text{LaFeAsO}$  and  $\text{SmFeAsO}$  compounds. *J. Magn. Magn. Mater.* **2009**, *321*, 3024–3030. [[CrossRef](#)]
24. Fiamozzi Zignani, C.; De Marzi, G.; Grimaldi, G.; Leo, A.; Guarino, A.; Vannozzi, A.; della Corte, A.; Pace, S. Fabrication and Physical Properties of Polycrystalline Iron-Chalcogenides Superconductors. *IEEE Trans. Appl. Supercond.* **2017**, *27*, 1–5. [[CrossRef](#)]
25. Cheng, Z.; Liu, S.; Dong, C.; Huang, H.; Li, L.; Zhu, Y.; Awaji, S.; Ma, Y. Effects of core density and impurities on the critical current density of  $\text{CaKFe}_4\text{As}_4$  superconducting tapes. *Supercond. Sci. Technol.* **2019**, *32*, 105014. [[CrossRef](#)]
26. Pak, C.; Su, Y.F.; Collantes, Y.; Tarantini, C.; Hellstrom, E.E.; Larbalestier, D.C.; Kametani, F. Synthesis routes to eliminate oxide impurity segregation and their influence on intergrain connectivity in K-doped  $\text{BaFe}_2\text{As}_2$  polycrystalline bulks. *Supercond. Sci. Technol.* **2020**, *33*, 084010. [[CrossRef](#)]
27. Fiamozzi Zignani, C.; De Marzi, G.; Corato, V.; Mancini, A.; Vannozzi, A.; Rufoloni, A.; Leo, A.; Guarino, A.; Galluzzi, A.; Nigro, A.; et al. Improvements of high-field pinning properties of polycrystalline  $\text{Fe}(\text{Se},\text{Te})$  material by heat treatments. *J. Mater. Sci.* **2019**, *54*, 5092–5100. [[CrossRef](#)]
28. Pyon, S.; Suwa, T.; Tamegai, T.; Takano, K.; Kajitani, H.; Koizumi, N.; Awaji, S.; Zhou, N.; Shi, Z. Improvements of fabrication processes and enhancement of critical current densities in  $(\text{Ba},\text{K})\text{Fe}_2\text{As}_2$  HIP wires and tapes. *Supercond. Sci. Technol.* **2018**, *31*, 055016. [[CrossRef](#)]
29. Dew-Hughes, D. Flux pinning mechanisms in type II superconductors. *Philos. Mag.* **1974**, *30*, 293–305. [[CrossRef](#)]
30. Zhang, L.; Qiao, Q.; Xu, X.B.; Jiao, Y.L.; Xiao, L.; Ding, S.Y.; Wang, X.L. Surface barrier and bulk pinning in MTG  $\text{YBaCuO}$ . *Phys. C Supercond. Appl.* **2006**, *445–448*, 236–239. [[CrossRef](#)]
31. Bean, C.P. Magnetization of hard superconductors. *Phys. Rev. Lett.* **1962**, *8*, 250–253. [[CrossRef](#)]
32. Bean, C.P. Magnetization of High-Field Superconductors. *Rev. Mod. Phys.* **1964**, *36*, 31–39. [[CrossRef](#)]
33. Singh, S.J.; Cassidy, S.J.; Bristow, M.; Blundell, S.J.; Clarke, S.J.; Coldea, A.I. Optimization of superconducting properties of the stoichiometric  $\text{CaKFe}_4\text{As}_4$ . *Supercond. Sci. Technol.* **2019**, *33*, 025003. [[CrossRef](#)]
34. Griessen, R.; Hai-Hu, W.; Van Dalen, A.J.J.; Dam, B.; Rector, J.; Schnack, H.G.; Libbrecht, S.; Osquiguil, E.; Bruynseraede, Y. Evidence for mean free path fluctuation induced pinning in  $\text{YBa}_2\text{Cu}_3\text{O}_7$  and  $\text{YBa}_2\text{Cu}_4\text{O}_8$  films. *Phys. Rev. Lett.* **1994**, *72*, 1910–1913. [[CrossRef](#)]
35. Savvides, N. Flux creep and transport critical current density in high-Tc superconductors. *Phys. C Supercond.* **1990**, *165*, 371–376. [[CrossRef](#)]
36. Murakami, M.; Fujimoto, H.; Gotoh, S.; Yamaguchi, K.; Koshizuka, N.; Tanaka, S. Flux pinning due to nonsuperconducting particles in melt processed  $\text{YBaCuO}$  superconductors. *Phys. C Supercond.* **1991**, *185–189*, 321–326. [[CrossRef](#)]
37. Yeshurun, Y.; Malozemoff, A.P. Giant flux creep and irreversibility in an Y-Ba-Cu-O crystal: An alternative to the superconducting-glass model. *Phys. Rev. Lett.* **1988**, *60*, 2202–2205. [[CrossRef](#)]
38. Jackson, D.J.C.; Das, M.P. Melting of the flux line lattice. *Supercond. Sci. Technol.* **1996**, *9*, 713–727. [[CrossRef](#)]

39. Yom, S.S.; Hahn, T.S.; Kim, Y.H.; Chu, H.; Choi, S.S. Exponential temperature dependence of the critical transport current in Y-Ba-Cu-O thin films. *Appl. Phys. Lett.* **1989**, *54*, 2370. [[CrossRef](#)]
40. Hsiang, T.Y.; Finnemore, D.K. Superconducting critical currents for thick, clean superconductor—normal-metal—superconductor junctions. *Phys. Rev. B* **1980**, *22*, 154–163. [[CrossRef](#)]
41. Blatter, G.; Feigel'Man, M.V.; Geshkenbein, V.B.; Larkin, A.I.; Vinokur, V.M. Vortices in high-temperature superconductors. *Rev. Mod. Phys.* **1994**, *66*, 1125–1388. [[CrossRef](#)]
42. Polat, A.; Sinclair, J.W.; Zuev, Y.L.; Thompson, J.R.; Christen, D.K.; Cook, S.W.; Kumar, D.; Chen, Y.; Selvamanickam, V. Thickness dependence of magnetic relaxation and E-J characteristics in superconducting (Gd-Y)-Ba-Cu-O films with strong vortex pinning. *Phys. Rev. B* **2011**, *84*, 024519. [[CrossRef](#)]
43. Plain, J.; Puig, T.; Sandiumenge, F.; Obradors, X.; Rabier, J. Microstructural influence on critical currents and irreversibility line in melt-textured YBa<sub>2</sub>Cu<sub>3</sub>O<sub>7-x</sub> reannealed at high oxygen pressure. *Phys. Rev. B* **2002**, *65*, 104526. [[CrossRef](#)]
44. Nelson, D.R.; Vinokur, V.M. Boson localization and correlated pinning of superconducting vortex arrays. *Phys. Rev. B* **1993**, *48*, 13060–13097. [[CrossRef](#)]
45. Hwa, T.; Le Doussal, P.; Nelson, D.R.; Vinokur, V.M. Flux pinning and forced vortex entanglement by splayed columnar defects. *Phys. Rev. Lett.* **1993**, *71*, 3545–3548. [[CrossRef](#)]
46. LeBlanc, D.; LeBlanc, M.A.R. Ac-loss valley in type-II superconductors. *Phys. Rev. B* **1992**, *45*, 5443–5449. [[CrossRef](#)]
47. Kim, Y.B.; Hempstead, C.F.; Strnad, A.R. Critical Persistent Currents in Hard Superconductors. *Phys. Rev. Lett.* **1962**, *9*, 306–309. [[CrossRef](#)]
48. Kim, Y.B.; Hempstead, C.F.; Strnad, A.R. Magnetization and Critical Supercurrents. *Phys. Rev.* **1963**, *129*, 528–535. [[CrossRef](#)]
49. Fietz, W.A.; Beasley, M.R.; Silcox, J.; Webb, W.W. Magnetization of Superconducting Nb-25%Zr Wire. *Phys. Rev.* **1964**, *136*, A335–A345. [[CrossRef](#)]
50. Watson, J.H.P. Magnetization of synthetic filamentary superconductors. B. The dependence of the critical current density on temperature and magnetic field. *J. Appl. Phys.* **1968**, *39*, 3406–3413. [[CrossRef](#)]
51. Xu, M.; Shi, D.; Fox, R.F. Generalized critical-state model for hard superconductors. *Phys. Rev. B* **1990**, *42*, 10773–10776. [[CrossRef](#)]
52. Shabbir, B.; Wang, X.; Ghorbani, S.R.; Shekhar, C.; Dou, S.; Srivastava, O.N. Hydrostatic pressure: A very effective approach to significantly enhance critical current density in granular iron pnictide superconductors. *Sci. Rep.* **2015**, *5*, 8213. [[CrossRef](#)]
53. Nazarova, E.; Balchev, N.; Nenkov, K.; Buchkov, K.; Kovacheva, D.; Zahariev, A.; Fuchs, G. Improvement of the superconducting properties of polycrystalline FeSe by silver addition. *Supercond. Sci. Technol.* **2015**, *28*, 125013. [[CrossRef](#)]
54. Hilgenkamp, H.; Mannhart, J. Grain boundaries in high-Tc superconductors. *Rev. Mod. Phys.* **2002**, *74*, 485–549. [[CrossRef](#)]
55. Dimos, D.; Chaudhari, P.; Mannhart, J. Superconducting transport properties of grain boundaries in YBa<sub>2</sub>Cu<sub>3</sub>O<sub>7</sub> bicrystals. *Phys. Rev. B* **1990**, *41*, 4038–4049. [[CrossRef](#)]
56. Katase, T.; Ishimaru, Y.; Tsukamoto, A.; Hiramatsu, H.; Kamiya, T.; Tanabe, K.; Hosono, H. Advantageous grain boundaries in iron pnictide superconductors. *Nat. Commun.* **2011**, *2*, 409. [[CrossRef](#)]
57. Galluzzi, A.; Polichetti, M.; Buchkov, K.; Nazarova, E.; Mancusi, D.; Pace, S. Evaluation of the intragrain critical current density in a multidomain FeSe crystal by means of dc magnetic measurements. *Supercond. Sci. Technol.* **2015**, *28*, 115005. [[CrossRef](#)]